NASA TECHNICAL NOTE

NASA TN D-4834

NASA TN D-4834

LOAN COPY: RETUR
AFWL (WLIL-2)
KIRTLAND AFB, N M

TECH LIBRARY KAFB, NM
0131635

EFFECTS OF ZINC CONCENTRATION ON OUTPUT OF ZINC-DOPED GERMANIUM DETECTORS

by Wilfred D. Hesketh

Langley Research Center

Langley Station, Hampton, Va.

NATIONAL AERONAUTICS AND SPACE ADMINISTRATION • WASHINGTON, D. C. • OCTOBER 1968

TECH LIBRARY KAFB, NM
0131635

NASA TN D-4834

EFFECTS OF ZINC CONCENTRATION ON OUTPUT OF ZINC-DOPED GERMANIUM DETECTORS

By Wilfred D. Hesketh

Langley Research Center
Langley Station, Hampton, Va.

NATIONAL AERONAUTICS AND SPACE ADMINISTRATION

For sale by the Clearinghouse for Federal Scientific and Technical Information
Springfield, Virginia 22151 – CFSTI price $3.00

EFFECTS OF ZINC CONCENTRATION ON OUTPUT OF ZINC-DOPED GERMANIUM DETECTORS

By Wilfred D. Hesketh
Langley Research Center

SUMMARY

The effects of dopant concentration on the operation of far infrared detectors were investigated both theoretically and experimentally.

The theoretical investigation shows that an optimum dopant concentration does exist in extrinsic quantum detectors. This optimum point will vary with changes in the host or dopant material. The optimum will also vary with changes in the integrating chamber used. A close examination of the integrating chamber must be conducted before it is possible to predict the operation or optimum dopant concentration of the detectors.

In the experimental investigation, an integrating chamber was constructed and evaluated for its characteristics. These characteristics, radiation loss coefficient due to reflections from the input port γ and radiation loss due to absorption by the integrating chamber walls δ, were then used in predicting the optimum dopant concentration of zinc-doped germanium. Ten detector pairs were produced from a single host crystal which was grown from a relatively dopant-free seed end and with increasing dopant concentration until twinning and shearing occurred. Two detectors were then cut from each of 10 different axial points along the crystal. This procedure produced 10 pairs of detectors of various dopant concentration with equal dopant concentration in the two detectors of each pair. The output of the detectors was measured, the measurement being normalized to the maximum value and plotted. These curves were then compared with similarly normalized theoretical curves. The optimum dopant concentration occurred as predicted but with a greater slope on each side of the optimum point than was predicted.

INTRODUCTION

Presently available quantum detectors will vary considerably in their operating characteristics. The characteristics in question may be responsivity or detectivity. These characteristics vary by a factor of two between detectors produced by a single company and by factors of 10 between similar detectors produced by various companies. These differences in operating characteristics may be due in part to variations in the dopant concentration in the detector elements.

A theoretical and experimental investigation has been conducted to determine the effects of dopant concentration on the relative response of a series of detectors. From the theoretical investigation, it can be seen that the number of photoionized carriers p will increase with increased dopant concentration to a point of complete photon absorption by the detector in a single pass. The number of thermally ionized carriers P will continually increase with dopant concentration. The output signal of the detector is a function of the ratio p/P; thus, the signal out will have an optimum dopant concentration.

The results of the theoretical investigation were then used to predict the optimum dopant concentration for zinc-doped germanium detectors in a well-defined integrating chamber.

Ten detector pairs of zinc-doped germanium, having dopant concentrations in the ranges from 10^{14} to 10^{17} parts per cm^3, were produced for the experimental investigation. Relative responsivities of the detectors were measured and the results are tabulated and compared with the theoretical analysis.

SYMBOLS

A,C,D	constants
a	principal quantum number
B	number of usable events per second produced by F_{sn}
c	speed of light
d	depth of detector, centimeter
E_a	energy level of acceptor, electron volts $(1.6 \times 10^{-19}$ joules)
E_c	energy level of conduction band, electron volts $(1.6 \times 10^{-19}$ joules)
E_f	Fermi energy level, electron volts $(1.6 \times 10^{-19}$ joules)
E_v	energy level of valence band, electron volts $(1.6 \times 10^{-19}$ joules)
F_i	number of photons incident on detector, photons/centimeter^2-micrometer-second)

F_D	number of photons entering the detector at $x = 0$, photons/centimeter^2-micrometer-second
F_o	number of photons entering the integrating chamber, photons/centimeter^2-micrometer-second
F_{sn}	total number of photons absorbed by the detector, photons/centimeter^2-micrometer-second
f	continuum oscillator strength
g	Gaunt factor
I_i	power intensity incident on detector, watts/centimeter^2
I_D	power intensity entering detector at $x = 0$, watts/centimeter^2
I_r	power intensity reflected by detector, watts/centimeter^2
I(x)	power intensity transmitted by a detector of depth x, watts/centimeter^2
k	Boltzmann's constant
l	length of detector, centimeters
M_a	dopant concentration, parts per centimeter^3
M_c	allowed density of states in conduction band, per centimeter^3
M_v	allowed density of states in valence band, per centimeter^3
$M(E_a)$	allowed density of states at acceptor level, per centimeter^3
N	number of thermally ionized electron carriers
n	number of reflected passes through detector by photons
P	number of thermally ionized free hole carriers produced by wanted dopant

P'	number of thermally ionized free hole carriers produced by unwanted impurities
p	number of photoionized free hole carriers
Q_R	response quantum efficiency of detector
q	electron charge, 1.60×10^{-19} coulomb
R_c	dark resistance of detector, ohms
R_c'	resistance of detector with signal applied, ohms

$\Delta R_c = -R_c + R_c'$, ohms

R_L	load resistor, ohms
S	photon capture cross section of dopant, centimeter^2
T	temperature, degrees Kelvin
V	bias voltage, volts
V_L	voltage across load resistor, volts
V_s	detector output signal voltage, volts
V_{sm}	normalized maximum detector output signal voltage
w	width of detector, centimeters
x	depth of penetration of photons into detector, centimeters
Z	charge on dopant ion
α	absorption coefficient of detector dopant
ϵ	energy of free electron, electron volts (1.6×10^{-19} joules)

λ	wavelength of photons, centimeters
γ	radiation loss coefficient due to reflections from input port
δ	radiation loss coefficient due to absorption by integrating chamber walls
ρ	reflection coefficient of detector
τ	free carrier lifetime, seconds
σ	conductivity, mhos
φ	absorption coefficient of detector impurities and lattice imperfections
μ_n	mobility of electrons in host material, centimeter^2/volt-second
μ_p	mobility of holes in host material, centimeter^2/volt-second

THEORETICAL INVESTIGATION

This paper will consider the thermally generated carriers and the change in the Fermi level for the case of acceptor level dopants. The theoretical results may be used for donor-type dopants if appropriate assumptions are made.

A photoconducting detector is generally operated in the circuit configuration shown in figure 1. Solving for the voltage across the load resistor

$$V_L = \frac{VR_L}{R_L + R_c} \tag{1}$$

If the small signal case is assumed, the signal voltage V_S can be given as the differentiation of equation (1) with respect to R_c. Maximizing V_S with respect to R_L gives $R_L = R_c$ and

$$V_S = -\frac{V}{4}\frac{\Delta R_c}{R_c} \tag{2}$$

The relation between the maximum signal voltage $(V_S)_{max}$ and the number of thermal and photoionized carriers can be found as follows:

$$\sigma = q\left(\mu_n N + \mu_p P\right) \tag{3}$$

If $P >> N$ which is the case for zinc-doped germanium is assumed,

$$\sigma = q\mu_p P$$

$$R_c = \frac{1}{q\mu_p P}\frac{l}{wd} \tag{4}$$

where

P	thermally ionized carriers
μ_p	carrier mobility
q	electron charge
l,w,d	length, width, and depth of detector, respectively

If there are a number of photoionized carriers p in the detector,

$$R_c' = \frac{1}{q\mu_p(P + p)}\frac{l}{wd} \tag{5}$$

$$\Delta R_c = -R_c + R_c' = \frac{1}{q\mu_p}\frac{l}{wd}\left(\frac{1}{P} - \frac{1}{P + p}\right)$$

$$\Delta R_c = \frac{-1}{q\mu_p}\frac{l}{wdP}\left(\frac{P}{P + p}\right) \tag{6}$$

Substituting R_c from equation (4) into equation (6) yields

$$\Delta R_c = -R_c\left(\frac{P}{P + p}\right) \tag{7}$$

Substituting equation (7) into equation (2) yields

$$V_S = \frac{V}{4}\left(\frac{P}{P + p}\right) \tag{8}$$

The number of thermally ionized impurities P is a function of dopant concentration M_a and operating temperature T and is given in reference 1 as

$$P = \frac{M(E_a)}{1 + e^{(E_a - E_f)/kT}} \tag{9}$$

where

$M(E_a)$ number of total available states at acceptor level

E_a energy level of acceptor impurities in electron volts

E_f Fermi energy level at temperature T and concentration level M_a

k Boltzmann's constant

T temperature, ^{o}K

The sign convention to be used in this paper is that the upper edge of the last valence band energy E_v is taken to be the reference value or zero. Any energy level from this point toward the conduction band is considered to be positive. The Fermi energy level E_f is a function of temperature T and dopant concentration M_a. If it is assumed that there are no unwanted impurities in the crystal, the Fermi level of an acceptor-type dopant concentration may be found from reference 1 to be

$$M_v e^{-(E_f - E_v)/kT} = M_c e^{-(E_c - E_f)/kT} + \frac{M(E_a)}{1 + e^{-(E_f - E_a)/kT}} \tag{10}$$

Equation (10) is valid only if $(E_f - E_v) > 3kT$. Since the dopants are considered to be acceptors only, the Fermi level will shift toward the valence band from its intrinsic position. Then solving equation (10) for E_f gives

$$-E_f \approx kT \log_e \left\{ \frac{-1 + \left[1 + 4 \frac{M(E_a)}{M_v} e^{E_a/kT} \right]^{1/2}}{2e^{E_a/kT}} \right\} \tag{11}$$

The minimum controlled dopant in a crystal structure is on the order of 10^{13} to 10^{14} parts per cm^3. Using this value as a minimum for $M(E_a)$ and the low-temperature case which reduces the thermally excited carriers gives

$$\left[4 \frac{M(E_a)}{M_v} e^{E_a/kT}\right]^{1/2} >> 1$$

Thus

$$-E_f \approx kT \log_e \left(\frac{M_v}{e^{E_a/kT}} \right)^{1/2} \left[M(E_a)\right]^{1/2} \tag{12}$$

For a given temperature and material,

$$E_f \approx -c - kT \log_e \left[M(E_a)\right]^{1/2} \tag{13}$$

Substituting into equation (9) gives

$$P = \frac{M(E_a)}{e} e^{E_a/kT} e^{c} \left[M(E_a)\right]^{1/2}$$

For any given temperature $e^{E_a/kT} e^{c}$ is a constant; thus,

$$P = D\left[M(E_a)\right]^{1/2} \tag{14}$$

for $P << M(E_a)$. The photoionized carriers p are proportional to the number of absorbed photons. The amount of radiation absorbed by the semiconductor will follow Bouguer's law of absorption, from reference 2, which is

$$I(x) = I_D e^{-\alpha x} \tag{15}$$

where

I_D incident power intensity minus reflected power intensity, $I_i - I_r$, watts/centimeter^2

α absorption coefficient of material

x distance in material at which $I(x)$ is measured

$I(x)$ transmitted power intensity

To calculate the number of ionized impurities, it is necessary to have the absorbed radiation and Bouguer's law in terms of photons:

$$F_i = A\lambda I_i$$

$$\frac{F(x)}{A\lambda} = \frac{F_D}{A\lambda} e^{-\alpha x}$$

where the constant A is the conversion factor given by Planck's constant h and the velocity of light c; therefore,

$$F(x) = F_D e^{-\alpha x} \tag{16}$$

where $F(x)$ is the transmitted photons.

The absorption coefficient of a doped semiconductor is small; therefore, the distance x must be made large to absorb all or most of the incident radiation. The distance x may be made large by either increasing the physical size of the sample or placing the sample in an integrating chamber. A physically large sample would reduce the resistance of the detector R_c below a reasonable value. The use of an integrating chamber, consisting of a spherical chamber with highly reflective walls, produces multiple reflections of the radiation through the detector and thus increases the effective sample depth while maintaining a reasonably high dark resistance.

The assumption used in calculating the operation of the integrating chamber is that all energy reflected from the inner surface of the chamber must pass through the detector sample before reaching another portion of the inner surface of the chamber. (See fig. 2.)

In the appendix it is shown that the total number of photons per second absorbed for n passes through the semiconductor sample F_{sn} is given by

$$F_{sn} = F_o(1 - \rho)\left(1 - e^{-\alpha x}\right)\left(\frac{1 - \left\{(1 - \gamma - \delta)\left[1 - (1 - \rho)\left(1 - e^{-\alpha x}\right)\right]\right\}^n}{1 - (1 - \gamma - \delta)\left[1 - (1 - \rho)\left(1 - e^{-\alpha x}\right)\right]}\right) \tag{17}$$

where

F_o photons entering chamber per second

γ loss coefficient of integrating chamber due to reflections from input port

δ absorption coefficient of integrating chamber walls

ρ reflection coefficient of sample

α absorption coefficient of sample

x sample thickness, d

Absorption mechanisms within the detector other than the production of free carriers will place the number of photons per second causing free carriers below the number of absorbed photons per second F_{sn} by the detectors response quantum efficiency Q_R. The quantum efficiency Q_R is defined in reference 3 as

$$Q_R = \frac{B}{F_{sn}} \tag{18}$$

where

F_{sn} total number of absorbed photons per second

B number of photons producing free carriers

From reference 4, the number of photoionized carriers p may be found by

$$p = Q_R F_{sn} \tau \tag{19}$$

where τ is the lifetime of the free excess majority carriers. Substituting equation (17) into equation (19)

$$p = Q_R \tau F_o (1 - \rho)\left(1 - e^{-\alpha x}\right)\left(\frac{1 - \left\{(1 - \gamma - \delta)\left[\rho + (1 - \rho)e^{-\alpha x}\right]\right\}^n}{1 - \left\{(1 - \gamma - \delta)\left[\rho + (1 - \rho)e^{-\alpha x}\right]\right\}}\right) \tag{20}$$

In all cases the multiple reflections and passes through the semiconductor material n will continue until all the energy is either absorbed by the chamber walls and semiconductor or lost through reflections out of the input port. Let K be the final reflection and absorption pass after which no energy remains. Therefore, the photons per second incident on the detector after K reflections $F_{i,K+1}$ is zero. From the appendix

$$F_{i(K+1)} \approx F_o(1 - \gamma - \delta)^k\left[1 - (1 - \rho)\left(1 - e^{-\alpha x}\right)\right]^k \approx 0$$

Thus,

$$\underset{n \to K}{\text{Limit}} \left\{(1 - \gamma - \delta)\left[\rho + (1 - \rho)e^{-\alpha x}\right]\right\}^n = 0 \tag{21}$$

and

$$p = \frac{Q_R \tau F_o(1 - \rho)\left(1 - e^{-\alpha x}\right)}{1 - (1 - \gamma - \delta)\left[\rho + (1 - \rho)e^{-\alpha x}\right]} \tag{22}$$

The term α in the exponential may be broken into two parts to differentiate between that absorption which produces free carriers and that which only produces heat.

$$\alpha = SM_a + \varphi \tag{23}$$

where

S photon capture cross-section area of dopant, centimeter^2

M_a dopant concentration, atoms per centimeter^3

φ absorption coefficient by means other than dopant impurities such as free-carrier absorption or phonon absorption

As long as $\varphi << SM_a$, the response quantum efficiency can be assumed to be unity. If φ becomes appreciable compared with SM_a, absorption will increase but the number of usable events will not; thus, Q_R will decrease. Equations (17) and (18) show that for a constant φ and the lower dopant concentrations M_a, α is reduced; thus the response quantum efficiency will be less than that at the higher concentrations. Substituting equation (23) into equation (22) gives

$$p = \frac{Q_R \tau F_o (1 - \rho)\left(1 - e^{-SM_a x} e^{-\varphi x}\right)}{1 - (1 - \gamma - \delta)\left[\rho + (1 - \rho) e^{-SM_a x} e^{-\varphi x}\right]} \tag{24}$$

From equation (8),

$$V_{s,max} = \frac{V}{4}\left(\frac{p}{P + p}\right)$$

and from the assumption of the small signal case $P >> p$

$$V_{s,max} = \frac{V}{4}\frac{p}{P}$$

$$V_{s,max} = \frac{V}{4} Q_R \tau \frac{F_{sK}}{P} \tag{25}$$

Normalizing $V_{s,max}$ yields

$$V_{sm} = \frac{F_{sK_1}/P_1}{F_{sK_2}/P_2} \tag{26}$$

but from equation (14)

$$\frac{P_1}{P_2} = \left[\frac{M(E_a)_1}{M(E_a)_2}\right]^{1/2}$$

Thus

$$V_{sm} = \frac{F_{sK_1}}{F_{sK_2}}\left[\frac{M(E_a)_2}{M(E_a)_1}\right]^{1/2} \tag{27}$$

where the subscripts 1 and 2 denote different dopant concentrations, subscript 1 denoting that concentration which gives the maximum signal voltage.

Normalized curves of $V_{s,max}$ as a function of dopant concentration are shown in figure 3 with capture cross sections as a parameter and φ equal to zero and in figure 4 with integrating chamber losses as a parameter. The integrating chamber losses are given by the losses from the input port γ and the wall absorption coefficient δ. Variations in reflectance of the detector material have negligible effect on the position of the curve peak. It can be seen from figures 3 and 4 that there is an optimum dopant concentration for the maximum detector output. This optimum concentration level is not necessarily the maximum dopant that the host crystal can contain. The optimum point can be shifted toward the maximum dopant level by placing the detector in an integrating chamber with high losses or increasing the physical depth of the detector. Neither of these techniques will optimize the overall performance of the detector.

EXPERIMENTAL INVESTIGATION

The specifications for the series of detectors required 10 detector pairs produced from the same host crystal. The dopant concentration was to vary from zero dopant at the seed end of the crystal to maximum dopant just prior to twinning and shearing at the final axial cut. Doping was accomplished in a typical closed-system type-three zone furnace. (See fig. 5.) As the crystal molten zone was moved along the axis, the vapor pressure of the zinc was continually increased by increasing the temperature of the zinc. This increased vapor pressure produced variations in the dopant concentration along the axis of the host crystal. The detectors were then cut from the large doped crystal, two detectors being cut from each axial point selected. The points were chosen to produce 10 detector pairs, each pair having two detectors of equal dopant concentration and each consecutive pair having a higher dopant concentration. The dopant concentration for each pair was determined from Hall coefficient measurements by the manufacturer and is given in table I. The detectors were cut to 2 mm by 3 mm by 5 mm. One of the

TABLE I.- DOPANT CONCENTRATION OF THE TEST DETECTORS

Detector pair	Dopant concentration, M_a, parts per cubic centimeter	Available sites at the acceptor level, $M(E_a)$ (*)
1	6×10^{13}	1.2×10^{14}
2	5×10^{14}	1.0×10^{15}
3	8×10^{14}	1.6×10^{15}
4	2.1×10^{15}	4.2×10^{15}
5	5×10^{15}	1.0×10^{16}
6	6.5×10^{15}	1.3×10^{16}
7	2.2×10^{16}	4.4×10^{16}
8	4.3×10^{16}	8.6×10^{16}
9	6.5×10^{16}	1.3×10^{17}
10	7×10^{16}	1.4×10^{17}

*The zinc dopant is a double acceptor and thus $M(E_a) = 2M_a$.

2- by 3-mm faces was mounted on a gold-plated mounting plate with indium solder. A thin gold wire was then soldered to the opposite face. Chemical etching was used to remove surface damage and contaminants.

An integrating sphere was produced by boring with a spherical routing tool into two brass plates. Extreme care was used to produce a smooth surface and two well-matched hemispheres. A mismatch or a rough surface would have increased the losses in the sphere. After routing, the worked surface was smoothed by using a grinding compound and a stainless-steel ball as a lapping tool. The finished surfaces were then plated with silver by vacuum deposition. A flat brass plate was also lapped smooth and silver plated at the same time to produce a witness sample for tests. An entrance port was made on one side of the chamber and an indentation and opening were made to mount the detectors inside the integrating chamber. The reflectance of the silver coating on the witness plate was measured with an infrared spectrophotometer. The reflectance of the coating varied from 97 percent at 2 micrometers to 99.5 percent at 18 micrometers. The average reflectance over this range was approximately 98 percent and results in a δ of 0.02. The diameter of the integrating sphere was 0.394 inch and the diameter of the input port was 0.168 inch; these measurements result in a γ of 0.0455. Figure 6 is a photograph of the integrating chamber. A calibrated resistor was mounted in the brass block of the chamber mass to monitor the temperature of the detector and block in liquid helium. Because of heat loading, the temperature stabilized out at approximately 6.5° K. The capture cross section area S for zinc was calculated by using the following relationship from reference 5:

$$S = 8.067 \times 10^{-18} \frac{df}{d\epsilon}$$

where it was assumed that the differentials of continuum oscillator strength $df/d\epsilon$ do not vary over the frequency range used in the test from that of the absorption edge and are given by $0.98014 \frac{ag}{Z^2}$ where

a principal quantum number 4 for zinc

g Gaunt factor of 2.02 for the whole continuum

Z charge on the upper ion

From this S is found to be 1.6×10^{-17} cm^2.

Radiation at wavelengths of 2 micrometers or shorter had to be cut off from the detector to eliminate the intrinsic excitation of carriers in the germanium. The

absorption of short wavelengths by the germanium will occur within a few micrometers of the crystal surface because of the high α of an intrinsic material. The production of numerous free carriers within this small volume will effectively short out any resistance change due to the deeper penetrating longer wavelengths absorbed by the dopant. The blocking off of the shorter wavelength was accomplished by installing a germanium window at one end of a long tube while mounting the detector at the other end. To reduce the heat loss due to inserting the tube and detector into the liquid helium, the tube was constructed with thin-wall stainless-steel tubing. Brass ends were placed on the stainless-steel tube to permit easier working in the placing of the windows, detectors, and the sealing of the tube. It was necessary to evacuate the tube to eliminate the formation of frost on the inner side of the upper germanium window. To do this, a second window of pressed sintered zinc selenide was placed at the lower end of the tube just before the detector. To reduce the formation of frost on the outside of the germanium window, nitrogen gas was continually blown across the window to maintain a completely dry atmosphere for the window. Figures 7, 8, and 9 are photographs of the tube assembly. The windows limited the operation of the system to the 2- to 18-micrometer range.

A Nernst glower was used as the source of radiation. The glower was mounted at the focal point of a 3-inch mirror. (See fig. 10.) This system was then mounted over the germanium window and positioned for maximum output of the detector.

A chopper was placed between the source and the detector. This chopper provided the ac signal from the detector as well as the reference signal used in the systems measuring equipment. The chopper operated at 640 Hz. The measuring equipment was a phase-lock nanovoltmeter which provided maximum sensitivity for measuring the low signals.

By use of the previously measured values of $\gamma + \delta$ and calculated S, the solution of equation (22) with the theoretical curve of the relative signal out as a function of dopant concentration for the zinc-doped germanium detectors is shown in figure 11. The value of φ was assumed to be zero; this value gives a Q_R of unity. The lifetime τ was assumed to be constant in the region of optimum dopant concentration. The reflectance of germanium in the region of 2 to 20 micrometers was measured to be 0.28. The output of the detectors was measured in three different runs. Table II and figure 11 give the results.

It can be seen from figure 11 and table II that the optimum dopant concentration is between 1 and 3×10^{16} parts per cm^3 and not the maximum concentration of 10^{17} parts per cm^3.

TABLE II.- RELATIVE DETECTOR OUTPUT FOR THREE EXPERIMENTAL RUNS

Detector pair	Detector output for –			Dopant concentration, M_a, parts per cubic centimeter
	Run 1	Run 2	Run 3	
1	*	*	*	6×10^{13}
2	*	*	*	5×10^{14}
3	*	*	*	8×10^{14}
4	0.018	0.028	0.019	2.1×10^{15}
5	.048	.037	.024	5×10^{15}
6	.073	.078	.055	6.5×10^{15}
7	1	1	1	2.2×10^{16}
8	.466	.642	.58	4.3×10^{16}
9	.434	.52	.477	6.5×10^{16}
10	*	*	*	7×10^{16}

*Insufficient output to detect.

DISCUSSION OF RESULTS

Figure 11 shows the theoretical and experimental results of the study. The peak or optimum dopant concentration is that predicted. The experimental curve shows a greater slope on both sides of the peak. The increase in the slope at the lower concentration levels can be accounted for by an increased φ, which was assumed to be zero, and by adding in a constant value of thermally ionized carriers P' because of unwanted impurities which have a lower energy than the dopant. The constant P' could be of small enough value to be negligible at the higher dopant levels and still be the predominant carrier at the lower levels of concentration. By the same token, an increase in φ would cause a constant absorption factor to exist in equation (22). This absorption could be the predominant factor at the lower concentration levels, and would thus result in a lower Q_R at these lower levels.

The increase in the slope at the higher concentration levels may be due to a decrease in the lifetime of the carriers at these higher levels. The higher levels of dopant concentration increases the number of recombination centers within the material either from the increased impurities due to the relatively high impurity content of the

dopant or from an increased number of dislocations and imperfections in the lattice structure of the crystal due to the increased concentration of dopant. It is more likely to be a combination of these factors.

CONCLUDING REMARKS

A theoretical and experimental investigation has been conducted to determine the effect of dopant concentration on the output of a semiconductor infrared detector. The theoretical investigation has shown that an optimum dopant concentration does exist which is less than the maximum dopant level that can be obtained in zinc-doped germanium. The experimental investigation has agreed with the theory in that the maximum detector output was obtained at the predicted dopant concentration.

This study has shown in one case that it is possible to predict an optimum level of dopant concentration for extrinsic detectors. It also shows a possible reason for variations in the operation of commercially available detectors. With closer control of the detector dopant level, some of the variations in detector operating characteristics may be eliminated.

Langley Research Center,
National Aeronautics and Space Administration,
Langley Station, Hampton, Va., June 12, 1968,
125-17-02-08-23.

APPENDIX

DERIVATION OF NUMBER OF PHOTONS ABSORBED

In this appendix the number of photons per second absorbed by the detector in a spherical integrating chamber is derived. The symbols used in this appendix are:

F_r	photons per second reflected by detector
F_o	photons per second entering sphere
F_{an}	photons per second absorbed during nth pass through detector
F_{in}	photons per second incident on detector after $n - 1$ reflections in sphere
F_{rn}	photons per second reflected during nth pass through detector
F_{sn}	total photons per second absorbed for n passes through detector
F_{Tn}	photons per second transmitted by detector during nth pass through detector
r_p	radius of input port of sphere
r_s	radius of sphere
x	detector thickness
α	absorption coefficient of detector
γ	radiation loss coefficient due to reflection from input port
δ	radiation loss coefficient due to absorption by sphere walls
ρ	reflection coefficient of detector

In the following derivation, it is assumed that the order of events is such that the nth pass through the detector is followed by the nth reflection of the radiation from the integrating chamber wall. The photons per second reflected by the detector on pass n are

APPENDIX

$$F_{rn} = \rho F_{in} \tag{A1}$$

The photons per second transmitted through the detector on the nth pass are

$$F_{Tn} = (1 - \rho)F_{in}e^{-\alpha x} \tag{A2}$$

The number of photons per second absorbed by the detector on the first pass through the detector material is the incident photons per second minus the sum of reflected and transmitted photons per second and is given by F_{a1}

$$F_{a1} = F_{i1} - F_{r1} - F_{T1} = F_{i1} - \rho F_{i1} - (1 - \rho)F_{i1}e^{-\alpha x}$$

$$F_{a1} = F_{i1}(1 - \rho)\left(1 - e^{-\alpha x}\right) \tag{A3}$$

The photons per second incident on the first pass through the detector are equal to the photons per second entering the integrating chamber:

$$F_{i1} = F_o$$

$$F_{a1} = F_o(1 - \rho)\left(1 - e^{-\alpha x}\right) \tag{A4}$$

By use of equation (A1) and equation (A2) as was done to compute equation (A3), the number of photons per second absorbed on the second pass through the detector is

$$F_{a2} = F_{i2}(1 - \rho)\left(1 - e^{-\alpha x}\right) \tag{A5}$$

The incident photons per second for the second pass through the detector are given by

$$F_{i2} = \left(F_o - F_{a1}\right) - \gamma\left(F_o - F_{a1}\right) - \delta\left(F_o - F_{a1}\right) = \left(F_o - F_{a1}\right)(1 - \gamma - \delta)$$

where the term γ is the coefficient of energy loss due to reflectance out of the input port. It is assumed that a point source of light existed at the center of the integrating sphere; then the loss factor γ is the ratio of the area of the input port to the area of the sphere and is

$$\gamma = \frac{r_p^2}{4r_s^2} \tag{A6}$$

Substituting into equation (A4) gives

$$F_{i2} = \left[F_o - F_o(1 - \rho)\left(1 - e^{-\alpha x}\right)\right](1 - \gamma - \delta)$$

$$F_{i2} = F_o(1 - \gamma - \delta)\left[1 - (1 - \rho)\left(1 - e^{-\alpha x}\right)\right] \tag{A7}$$

Substituting equation (A7) into equation (A5) gives

$$F_{a2} = F_o(1 - \gamma - \delta)(1 - \rho)\left(1 - e^{-\alpha x}\right)\left[1 - (1 - \rho)\left(1 - e^{-\alpha x}\right)\right] \tag{A8}$$

The total photons per second absorbed after the second pass through the detector is the sum of the absorption for both individual passes and is

$$F_{s2} = F_{a1} + F_{a2} = F_o(1 - \rho)\left(1 - e^{-\alpha x}\right) + F_o(1 - \gamma - \delta)(1 - \rho)\left(1 - e^{-\alpha x}\right)\left[1 - (1 - \rho)\left(1 - e^{-\alpha x}\right)\right]$$

$$F_{s2} = F_o(1 - \rho)\left(1 - e^{-\alpha x}\right)\left\{1 + (1 - \gamma - \delta)\left[1 - (1 - \rho)\left(1 - e^{-\alpha x}\right)\right]\right\} \tag{A9}$$

In a similar manner for the third pass, equation (A5) takes the form

$$F_{a3} = F_{i3}(1 - \rho)\left(1 - e^{-\alpha x}\right) \tag{A10}$$

where the incident photons per second for the third pass are given by the photons incident on the second pass through the detector minus the photons lost by absorption or reflectance

$$F_{i3} = \left(F_{i2} - F_{a2}\right)(1 - \gamma - \delta)$$

Substituting this relation into equation (A7) and equation (A8) gives

$$F_{i3} = \left\{F_o(1 - \gamma - \delta)\left[1 - (1 - \rho)\left(1 - e^{-\alpha x}\right)\right] - F_o(1 - \gamma - \delta)(1 - \rho)\left(1 - e^{-\alpha x}\right)\left[1 - (1 - \rho)\left(1 - e^{-\alpha x}\right)\right]\right\}(1 - \gamma - \delta)$$

$$F_{i3} = \left\{F_o(1 - \gamma - \delta)\left[1 - (1 - \rho)\left(1 - e^{-\alpha x}\right)\right]\right\}\left[1 - (1 - \rho)\left(1 - e^{-\alpha x}\right)\right](1 - \gamma - \delta)$$

$$F_{i3} = F_o(1 - \gamma - \delta)^2\left[1 - (1 - \rho)\left(1 - e^{-\alpha x}\right)\right]^2 \tag{A11}$$

Substituting equation (A11) into equation (A10) gives

$$F_{a3} = F_o(1 - \rho)\left(1 - e^{-\alpha x}\right)(1 - \gamma - \delta)^2\left[1 - (1 - \rho)\left(1 - e^{-\alpha x}\right)\right]^2 \tag{A12}$$

The total absorbed photons per second after the third pass through the detector are the sum of all absorption for all three passes and is given by

$$F_{s3} = F_{s2} + F_{a3}$$

Substituting this relation into equation (A9) and equation (A12) yields

$$F_{s3} = F_o(1 - \rho)\left(1 - e^{-\alpha x}\right)\left\{1 + (1 - \gamma - \delta)\left[1 - (1 - \rho)\left(1 - e^{-\alpha x}\right)\right] + (1 - \gamma - \delta)^2\left[1 - (1 - \rho)\left(1 - e^{-\alpha x}\right)\right]^2\right\} \tag{A13}$$

As was done in equation (A4), the photons per second absorbed on the fourth pass through the detector are given by

$$F_{a4} = F_{i4}(1 - \rho)\left(1 - e^{-\alpha x}\right)$$

The incident photons per second on the detector are given by

$$F_{i4} = \left(F_{i3} - F_{a3}\right)(1 - \gamma - \delta) \tag{A14}$$

Substituting equation (A14) into equation (A10) gives

$$F_{i4} = F_{i3}(1 - \gamma - \delta)\left[1 - (1 - \rho)\left(1 - e^{-\alpha x}\right)\right]$$

Substituting this relation into equation (A11) gives

$$F_{i4} = F_o(1 - \gamma - \delta)^2\left[1 - (1 - \rho)\left(1 - e^{-\alpha x}\right)\right]^2(1 - \gamma - \delta)\left[1 - (1 - \rho)\left(1 - e^{-\alpha x}\right)\right]$$

$$F_{i4} = F_o(1 - \gamma - \delta)^3\left[1 - (1 - \rho)\left(1 - e^{-\alpha x}\right)\right]^3 \tag{A15}$$

Substituting equation (A15) into equation (A14) gives

$$F_{a4} = F_o(1 - \rho)\left(1 - e^{-\alpha x}\right)(1 - \gamma - \delta)^3\left[1 - (1 - \rho)\left(1 - e^{-\alpha x}\right)\right]^3 \qquad \text{(A16)}$$

The total absorbed photons per second after the fourth pass is the sum of all absorptions for all four passes and is

$$F_{s4} = F_{s3} + F_{a4}$$

Substituting this relation into equation (A13) and equation (A16) gives

$$F_{s4} = F_o(1 - \rho)\left(1 - e^{-\alpha x}\right)\left\{1 + (1 - \gamma - \delta)\left[1 - (1 - \rho)\left(1 - e^{-\alpha x}\right)\right] + (1 - \gamma - \delta)^2\left[1 - (1 - \rho)\left(1 - e^{-\alpha x}\right)\right]^2 + (1 - \gamma - \delta)^3\left[1 - (1 - \rho)\left(1 - e^{-\alpha x}\right)\right]^3\right\} \qquad \text{(A17)}$$

From the preceding work it can be seen that the total photon per second absorption can be described by a power series of the form

$$F_{sn} = F_o(1 - \rho)\left(1 - e^{-\alpha x}\right)\sum_{k=0}^{n-1}(1 - \gamma - \delta)^k\left[1 - (1 - \rho)\left(1 - e^{-\alpha x}\right)\right]^k$$

$$F_{sn} = F_o(1 - \rho)\left(1 - e^{-\alpha x}\right)\sum_{k=0}^{n-1}\left\{(1 - \gamma - \delta)\left[1 - (1 - \rho)\left(1 - e^{-\alpha x}\right)\right]\right\}^k \qquad \text{(A18)}$$

From reference 6

$$\sum_{k=0}^{i} X^k = \frac{1 - X^{i+1}}{1 - X}$$

where

$$X = (1 - \gamma - \delta)\left[1 - (1 - \rho)\left(1 - e^{-\alpha x}\right)\right]$$

Thus

$$F_{sn} = F_o(1 - \rho)\left(1 - e^{-\alpha x}\right)\left(\frac{1 - \left\{(1 - \gamma - \delta)\left[1 - (1 - \rho)\left(1 - e^{-\alpha x}\right)\right]\right\}^{n}}{1 - (1 - \gamma - \delta)\left[1 - (1 - \rho)\left(1 - e^{-\alpha x}\right)\right]}\right) \qquad \text{(A19)}$$

REFERENCES

1. Valdes, Leopoldo B.: The Physical Theory of Transistors. McGraw-Hill Book Co., Inc., c.1961.

2. Petritz, Richard L.: Fundamentals of Infrared Detectors. Proc. IRE, vol. 47, no. 9, Sept. 1959, pp. 1458-1467.

3. Jones, R. Clark: Quantum Efficiency of Detectors for Visible and Infrared Radiation. Vol. XI of Advances in Electronics and Electron Physics, L. Marton and Claire Marton, eds., Academic Press, Inc., 1959, pp. 87-183.

4. Rose, A.: Concepts in Photoconductivity and Allied Problems. Interscience Publishers, New York, N.Y., 1963.

5. Allen, C. W.: Astrophysical Quantities. Second ed., The Athlone Press (London), 1963.

6. Kunz, Kaiser S.: Numerical Analysis. McGraw-Hill Book Co., Inc., c.1957.

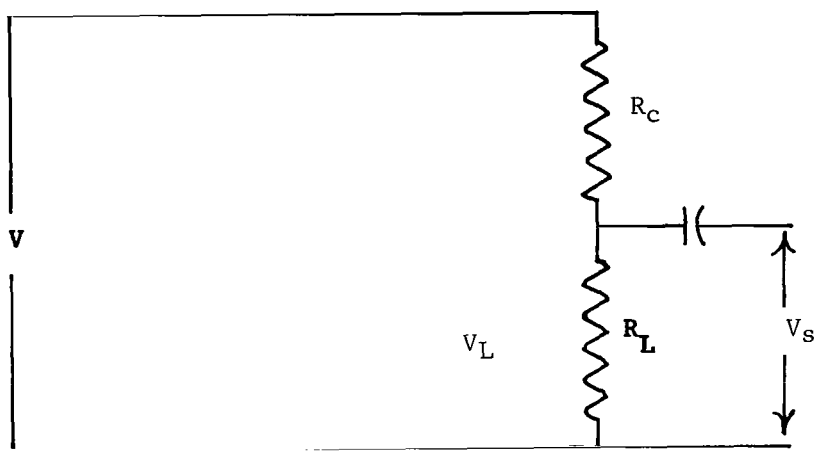

V Bias voltage source
V_S Signal voltage
R_C Photoconductor dark resistance
R_L Load resistor

Figure 1.- Detector circuit diagram.

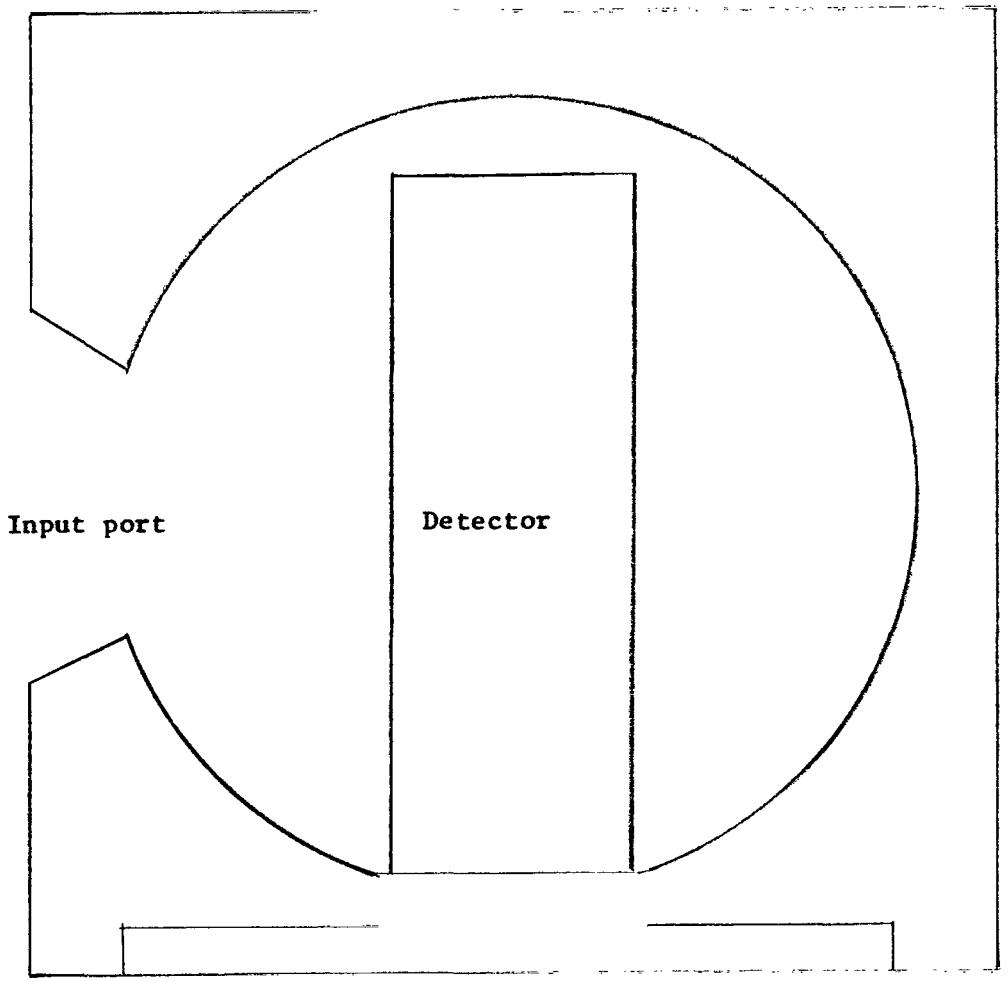

Figure 2.- Sketch of a spherical integrating chamber.

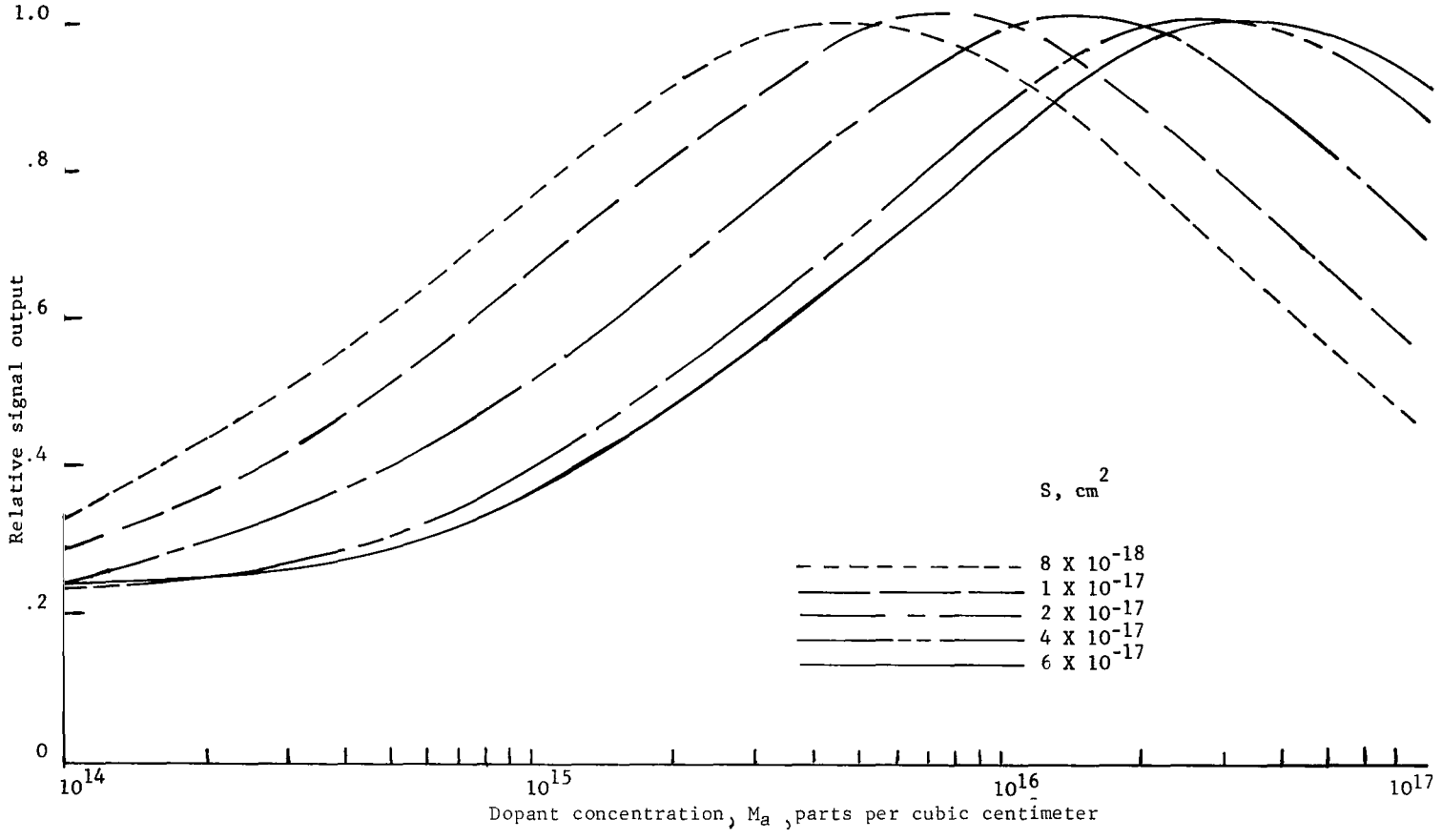

Figure 3.- Plot of signal voltage V_S as a function of dopant concentration with capture cross-section area S as a parameter. $\gamma + \delta = 0.04$; $x = 0.2$ cm; $\rho = 0.3$.

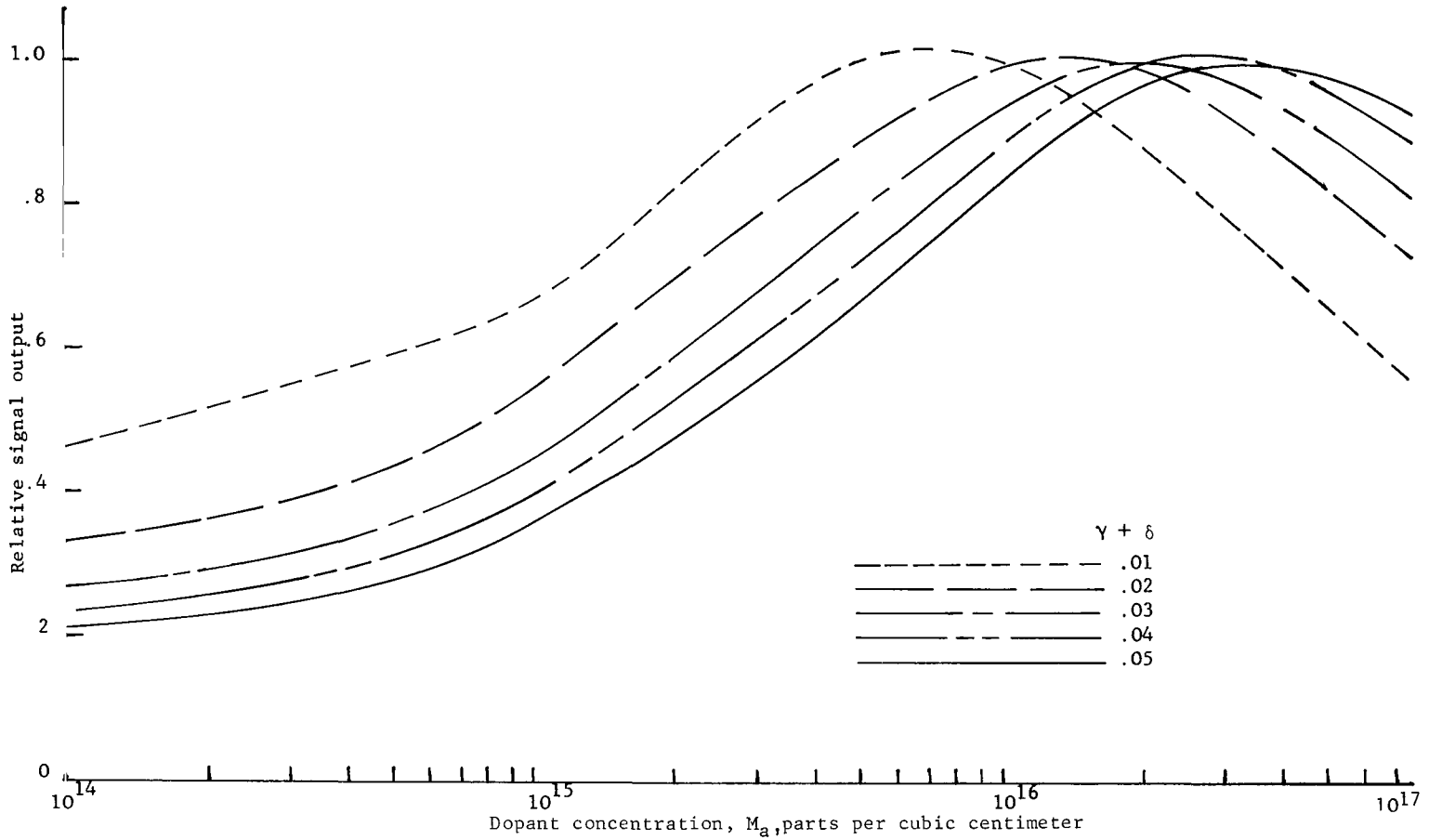

Figure 4.- Plot of signal voltage V_S as a function of dopant concentration with integration chamber losses γ and δ as parameters. $x = 0.2$ cm; $\rho = 0.3$; $S = 10^{-17}$ cm^2.

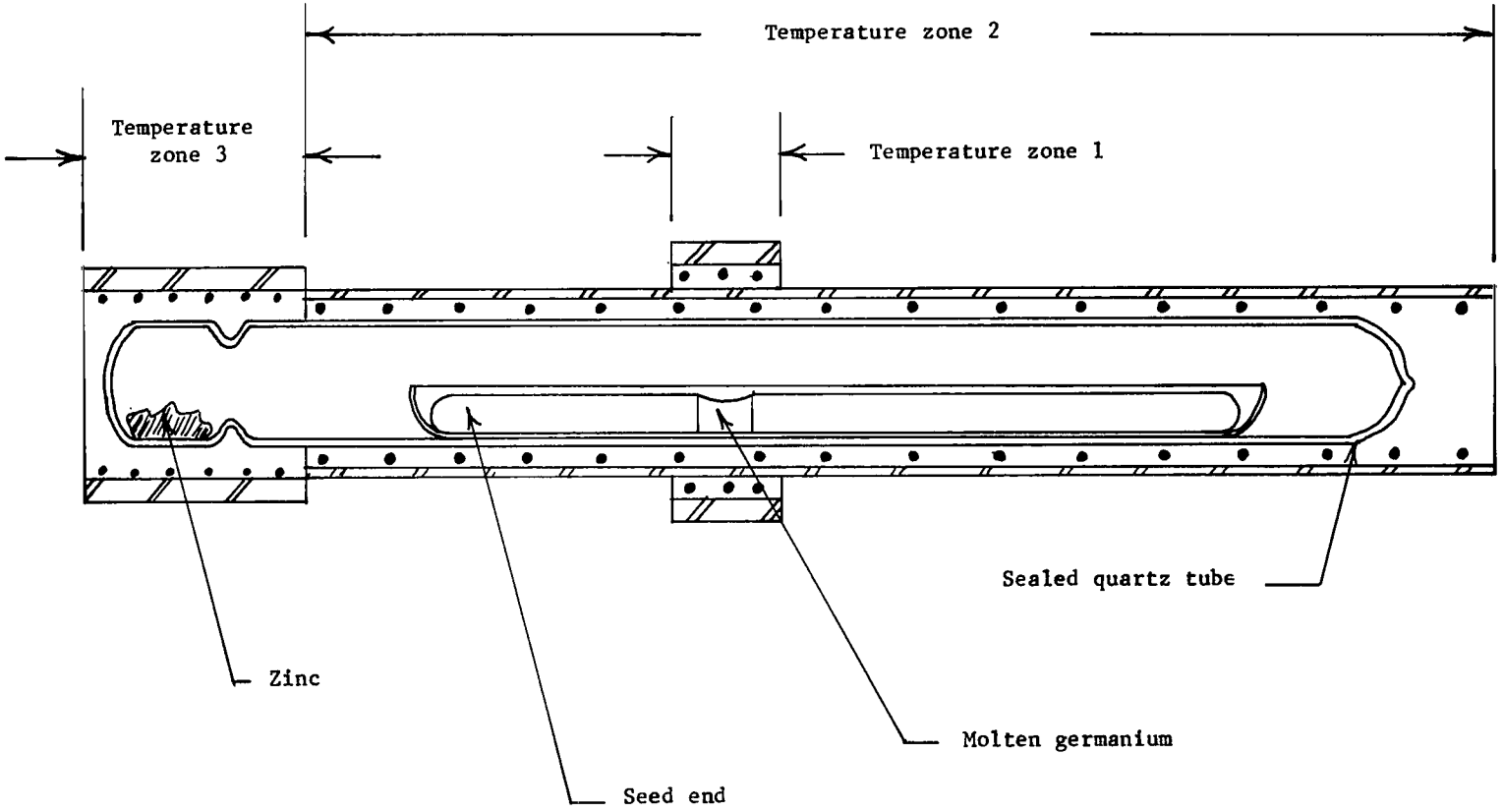

Figure 5.- Vapor doping furnace.

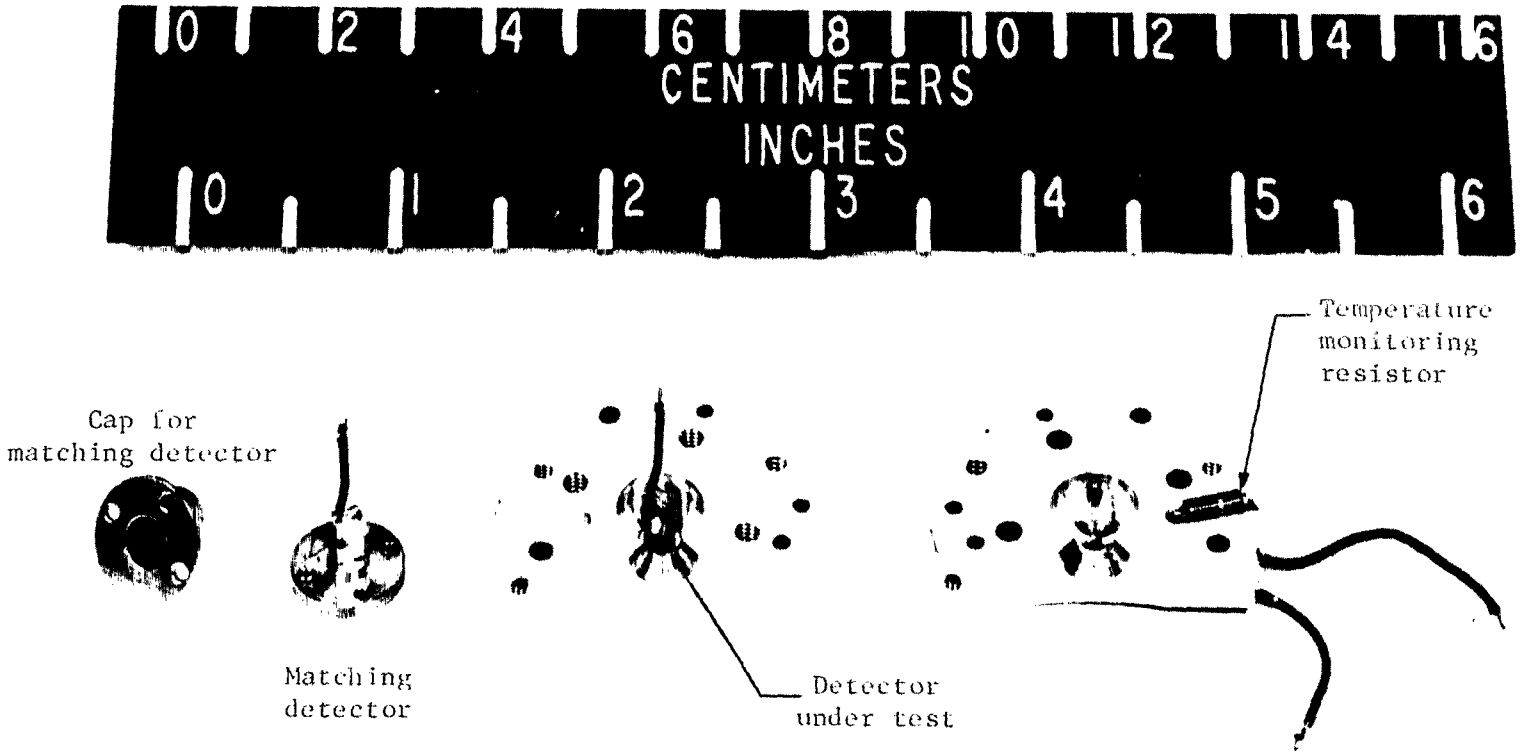

Figure 6.- Photograph of experimental integrating chamber.

I 66-9585.1

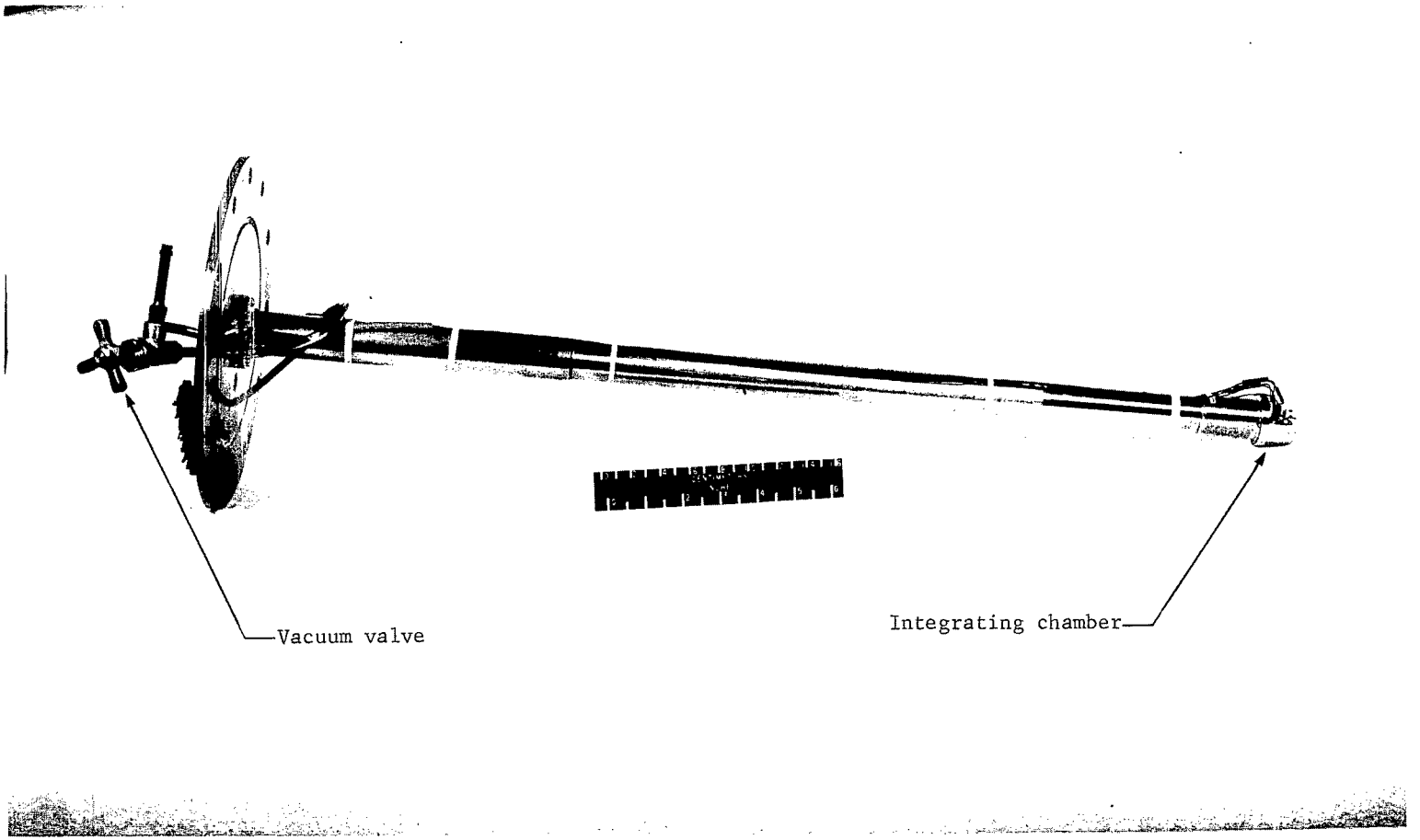

Figure 7.- Photograph of assembled cooling tube.

L-66-9581.1

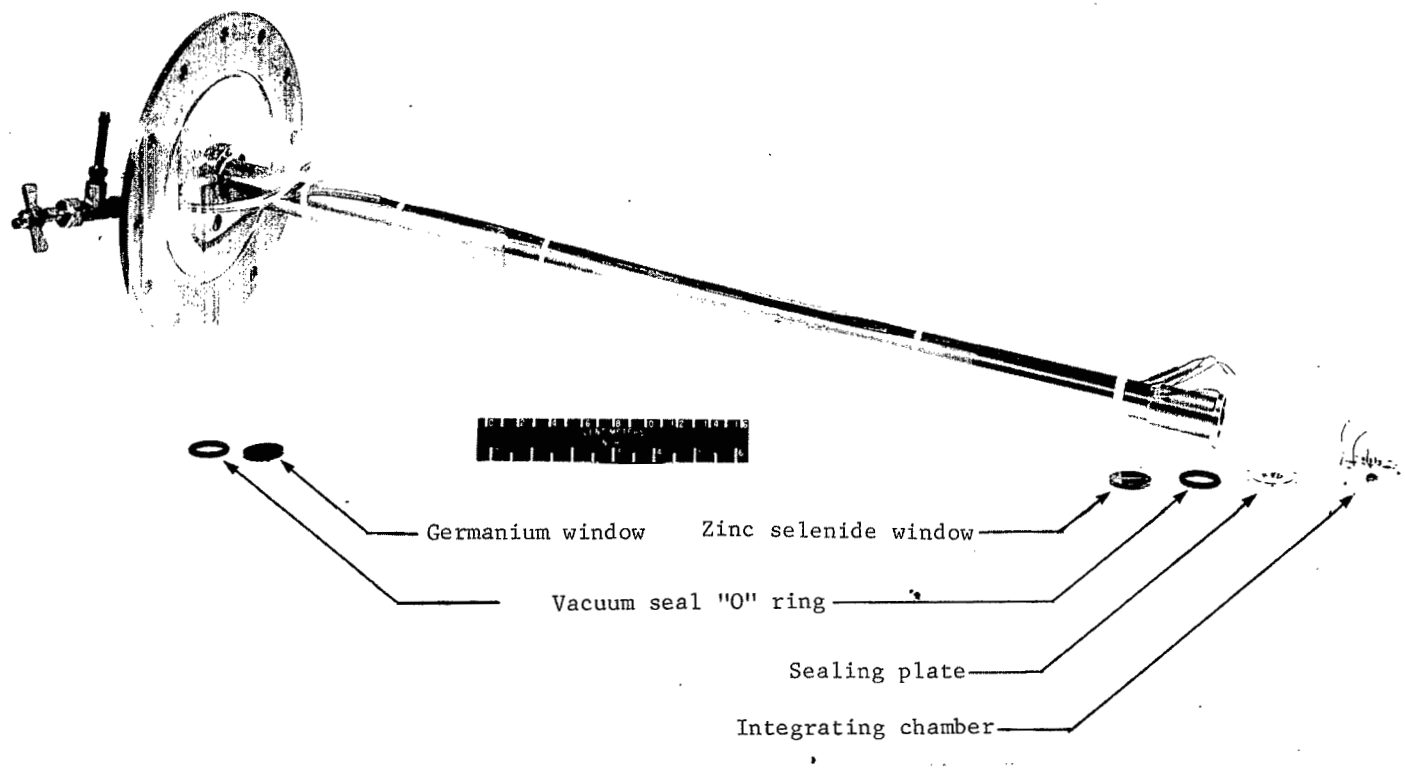

Figure 8.- Photograph of cooling tube disassembled.

L-66-9583.1

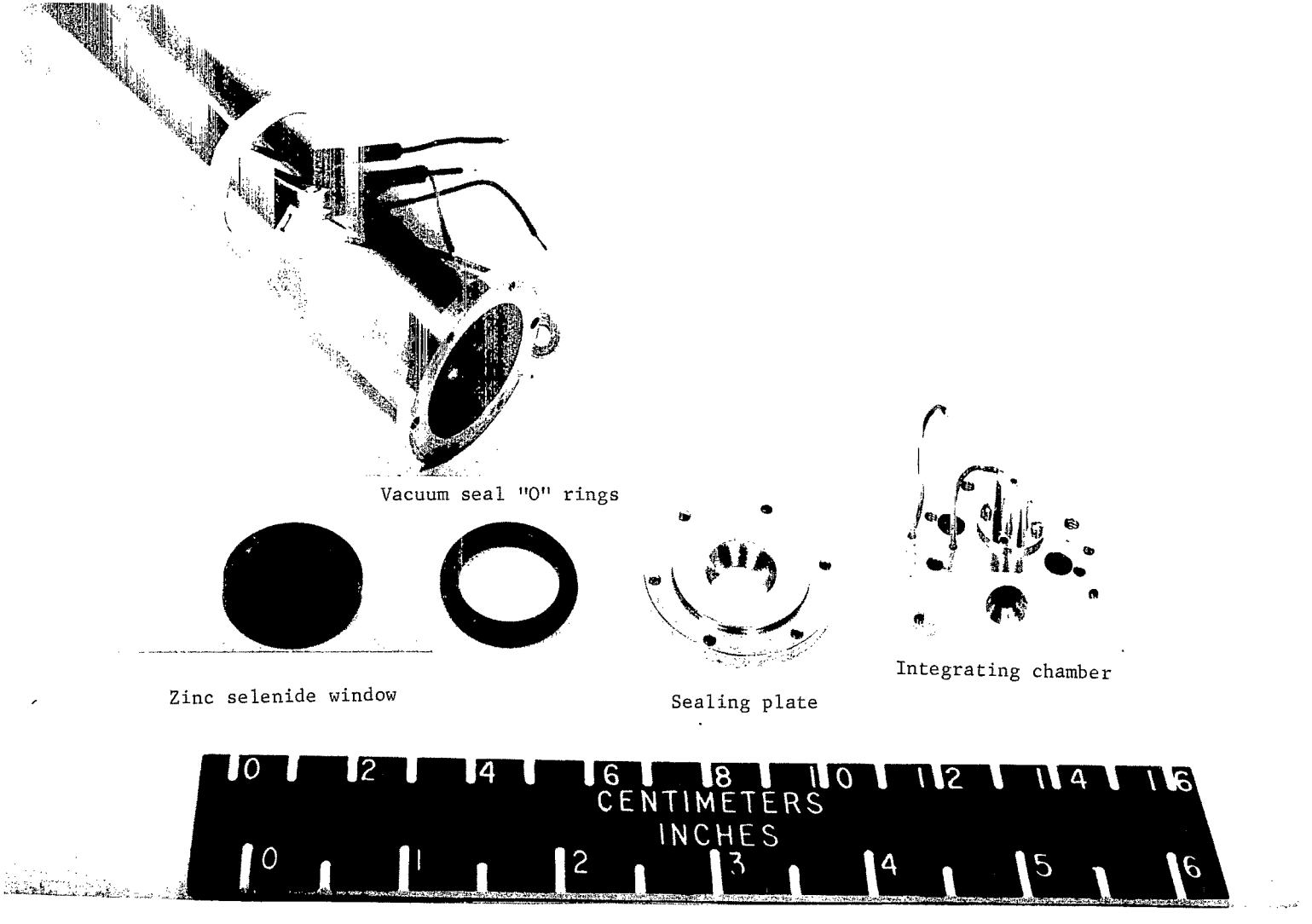

Figure 9.- Photograph of detector end of cooling tube.

L-66-9582.1

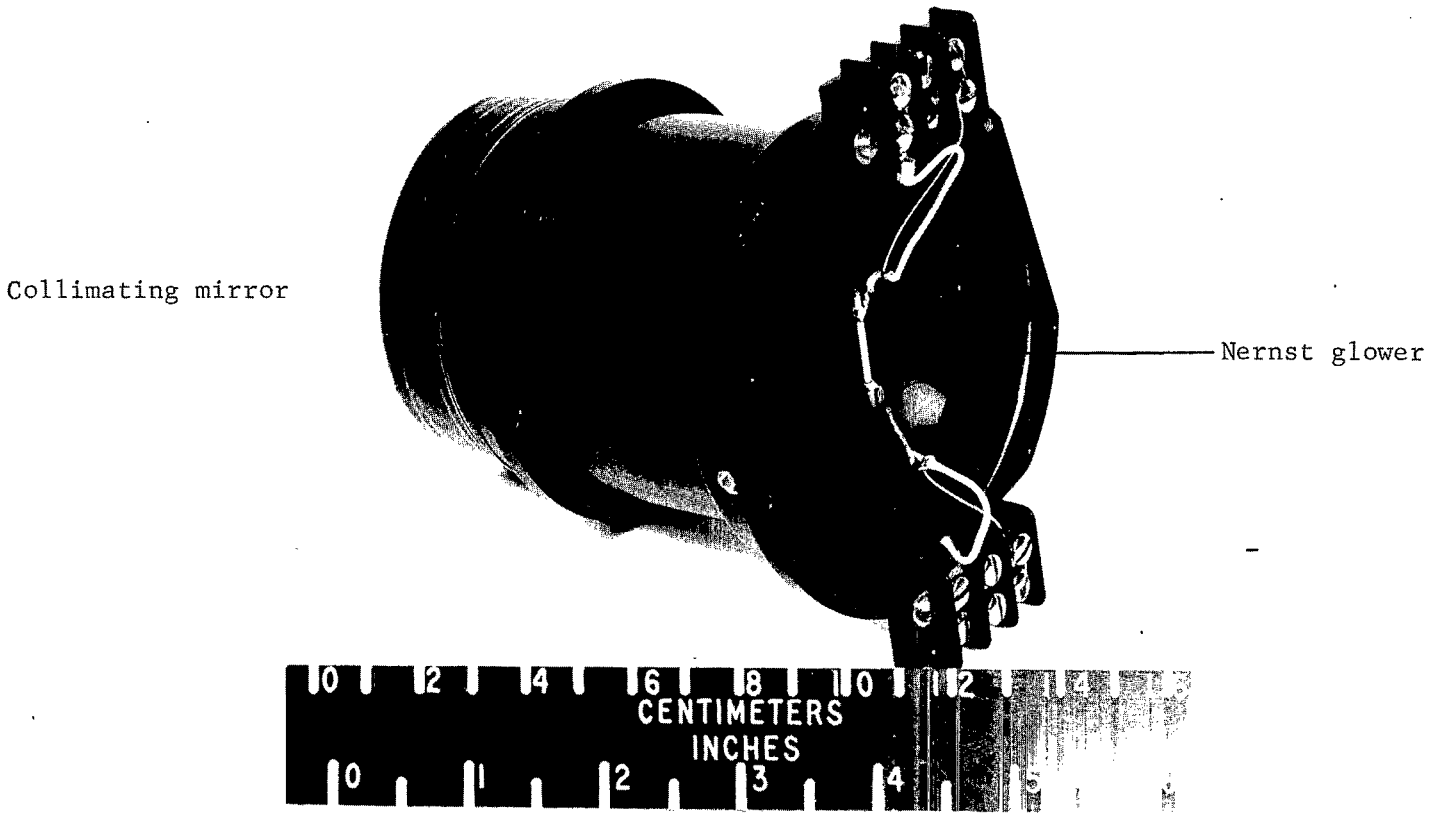

Figure 10.- Photograph of light source.

L-66-9584.1

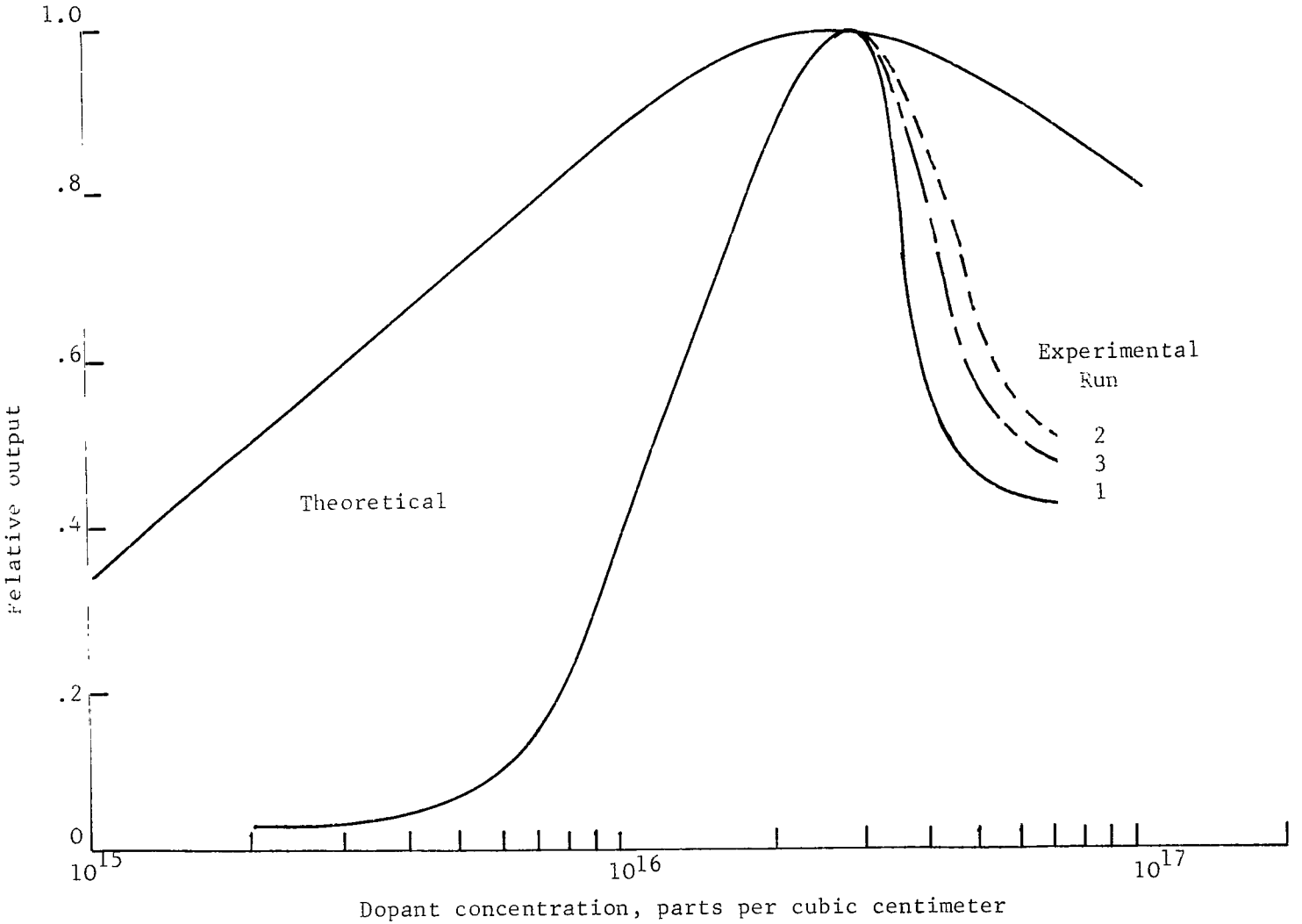

Figure 11.- Theoretical and experimental curves showing the normalized detector output as a function of dopant concentration.

NATIONAL AERONAUTICS AND SPACE ADMINISTRATION
WASHINGTON, D. C. 20546

OFFICIAL BUSINESS

FIRST CLASS MAIL

POSTAGE AND FEES PAID
NATIONAL AERONAUTICS AND
SPACE ADMINISTRATION

POSTMASTER: If Undeliverable (Section 158 Postal Manual) Do Not Return

"The aeronautical and space activities of the United States shall be conducted so as to contribute . . . to the expansion of human knowledge of phenomena in the atmosphere and space. The Administration shall provide for the widest practicable and appropriate dissemination of information concerning its activities and the results thereof."

—NATIONAL AERONAUTICS AND SPACE ACT OF 1958

NASA SCIENTIFIC AND TECHNICAL PUBLICATIONS

TECHNICAL REPORTS: Scientific and technical information considered important, complete, and a lasting contribution to existing knowledge.

TECHNICAL NOTES: Information less broad in scope but nevertheless of importance as a contribution to existing knowledge.

TECHNICAL MEMORANDUMS: Information receiving limited distribution because of preliminary data, security classification, or other reasons.

CONTRACTOR REPORTS: Scientific and technical information generated under a NASA contract or grant and considered an important contribution to existing knowledge.

TECHNICAL TRANSLATIONS: Information published in a foreign language considered to merit NASA distribution in English.

SPECIAL PUBLICATIONS: Information derived from or of value to NASA activities. Publications include conference proceedings, monographs, data compilations, handbooks, sourcebooks, and special bibliographies.

TECHNOLOGY UTILIZATION PUBLICATIONS: Information on technology used by NASA that may be of particular interest in commercial and other non-aerospace applications. Publications include Tech Briefs, Technology Utilization Reports and Notes, and Technology Surveys.

Details on the availability of these publications may be obtained from:

SCIENTIFIC AND TECHNICAL INFORMATION DIVISION

NATIONAL AERONAUTICS AND SPACE ADMINISTRATION

Washington, D.C. 20546